

Elongation and fluctuations of semi-flexible polymers in a nematic solvent

Z. Dogic,¹ J. Zhang,¹ A.W.C. Lau,¹ H. Aranda-Espinoza,² P. Dalhaimer,²
D.E. Discher,² P.A. Janmey,² T.C. Lubensky,¹ and A.G. Yodh¹

¹*Department of Physics and Astronomy, University of Pennsylvania, Philadelphia, Pennsylvania 19104*

²*Institute for Medicine and Engineering, University of Pennsylvania, Philadelphia, Pennsylvania 19104*

(Dated: October 3, 2003)

We directly visualize single polymers with persistence lengths ranging from $\ell_p = 0.05$ to $16 \mu\text{m}$, dissolved in the nematic phase of rod-like *fd* virus. Polymers with sufficiently large persistence length undergo a coil-rod transition at the isotropic-nematic transition of the background solvent. We quantitatively analyze the transverse fluctuations of semi-flexible polymers and show that at long wavelengths they are driven by the fluctuating nematic background. We extract both the Odijk deflection length and the elastic constant of the background nematic phase from the data.

PACS numbers: 61.30.-v, 64.70.Md, 82.35.Pq

Polymer coils in solution exhibit a variety of conformational and dynamical behaviors depending on many factors, including polymer concentration, polymer stiffness, solvent quality, solvent flow, and mechanical stress. Exciting recent experiments in this field have focused on disentanglement of single biopolymers in *isotropic* solutions [1] as a result of externally applied forces and solvent flow, and on transport of single biopolymers through networks of barriers [2] wherein conformational dynamics of the polymer play a critical role in affecting polymer separation. In this Letter, we explore the behavior of polymer coils in *anisotropic* solutions. In particular, we present the first experimental investigation of isolated semi-flexible polymers dissolved in a background nematic phase composed of aligned rod-like macromolecules. We show by direct visualization that semi-flexible biopolymers in the nematic phase assume an elongated rod-like configuration aligned with the background nematic director. The coil-rod transition of the biopolymer can thus be tuned by varying the concentration of rods in the background solvent so that the solvent undergoes an isotropic-nematic (I-N) phase transition. We quantitatively explore the fluctuations of semi-flexible polymers and find they cannot be described by a theory which treats the nematic background as a fixed external field [3].

Mixtures of semi-flexible polymers in lyotropic nematic suspensions exemplify an emerging class of complex fluids – hyper-complex fluids, such as nematic elastomers [4] and nematic emulsions [5], wherein two or more distinct components are combined to create systems that exhibit novel physical properties and functions. Understanding the polymer-nematic system may lead to new ideas about how to achieve a high alignment of biopolymers, complementary, for instance, to existing methods of DNA alignment [6]. Furthermore, since many biopolymers such as the actin filaments within the sarcomere and the neurofilaments within the axon are in an anisotropic, nematic-like environment [7], our investigation may shed light on the organization mechanisms within the cell.

We have used fluorescence microscopy to study four biopolymers in isotropic and nematic colloidal suspen-

TABLE I: The contour length L , the persistence length ℓ_p , and the diameter a of various polymers used in our experiments.

Polymer	L [μm]	ℓ_p [μm]	a [nm]	Ref.
λ -DNA	16	0.05	2	[18]
neurofilament	2-10	0.2	10	[19]
wormlike micelles	5-50	0.5	14	[17]
F-actin	2-20	16	7	[20]
<i>fd</i> virus	0.9	2.2	7	[13]

sions. This approach yields new information about dynamics and defects not readily accessible to traditional probes such as x-ray or neutron scattering [8]. In addition, we have developed a rotationally-invariant free energy for a single semiflexible polymer in a nematic matrix which generalizes the work in [9, 10], and enables us to extract the Odijk length [11] and the elastic constant of the liquid crystal. These first direct measurements of the Odijk deflection length λ allow us to quantify the length scale over which the polymer wanders before it is deflected back by the nematic director.

Our experiments employ an aqueous solution of rod-like *fd* viruses as a background nematic liquid crystal. This system has been studied extensively [12–14], and its phase behavior is well described by the Onsager theory for rods with hard core repulsion [15]. Another advantage of this system is its compatibility with most biopolymers. We use four different semi-flexible polymers, whose diverse physical parameters are listed in Table I. To directly visualize the polymers dissolved in the nematic background, we fluorescently labelled each polymer: DNA was labelled with YOYO-1 (Molecular Probes, Eugene OR), neurofilaments with succinimidyl rhodamine B [16], F-actin filaments with rhodamine-phalloidin (Sigma, St. Louis MO), and wormlike micelles with PKH26 dye (Sigma, St. Louis MO) which preferentially partitions into the hydrophobic core of the micelle. Since DNA, neurofilaments, and actin are all negatively charged, we expect that they are stable in a suspension of negatively charged *fd* viruses. Wormlike micelles are ster-

ically stabilized with a neutral PEO brush layer, which does not interact with *fd* virus or other proteins [13, 17].

Bacteriophage *fd* was grown and dialyzed against a phosphate buffer as previously described (150 mM KCl, 20 mM phosphate, 2 mM MgCl₂, pH=7.0) [13]. Samples were prepared by mixing a small amount of polymer with *fd* solution at different concentrations and were placed between a coverslip and a glass slide. A chamber with a thickness of $\sim 50 \mu\text{m}$ was made by using a stretched parafilm as a spacer. Samples sealed with optical glue (Norland Products, Cranbury, NJ) were allowed to equilibrate until no drift was visually detectable. To reduce

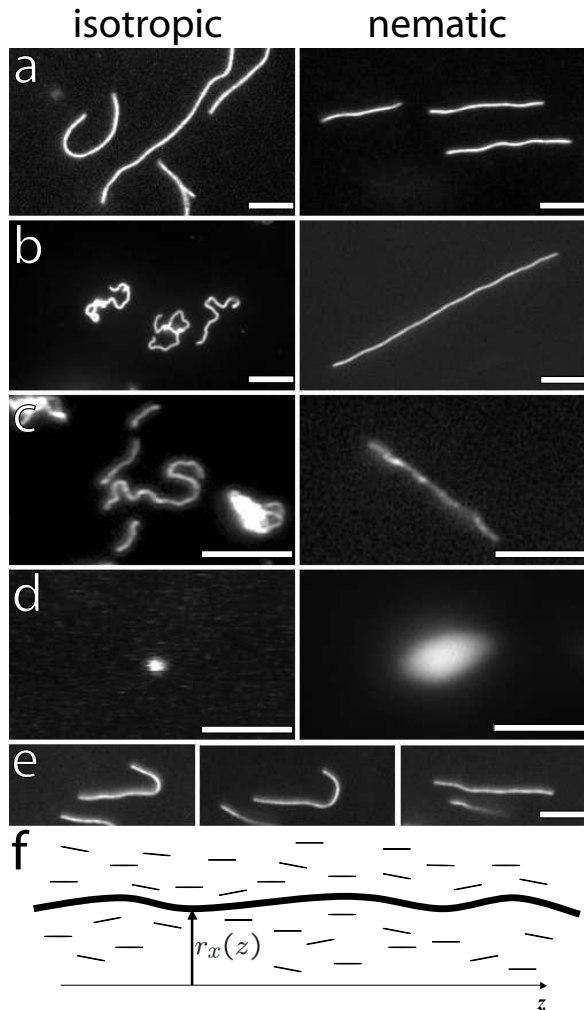


FIG. 1: Images of fluorescently labelled biopolymers in the isotropic (left) and nematic (right) phase of *fd* virus. Figures (a)-(d) are, respectively, the images of actin, wormlike micelles, neurofilaments, and DNA. The polymers in an isotropic solution are confined by a thin chamber thus making the samples quasi two dimensional. (e) A sequence of images illustrating an actin filament escaping from a hairpin defect. The scale bar is $5 \mu\text{m}$. (f) Schematic of a biopolymer in the background nematic field; the conformation of the polymer is parameterized by $\mathbf{R}(z) = \{r_x(z), r_y(z), z\}$. The nematic director points along the z -axis.

photobleaching, we added anti-oxygen solution (2 mg/ml glucose, 360 U/ml catalase, 0.25 vol% mercaptoethanol, 8 U/ml glucose oxidase). All samples were imaged with a fluorescence microscope (Leica IRBE) equipped with a 100x oil-immersion objective and a 100 W mercury lamp. Images were taken with a cooled CCD camera (CoolSnap HQ, Roper Scientific), which was focused at least $5 \mu\text{m}$ away from the surface to minimize possible wall effects.

Figure 1 displays a series of pictures that summarize our qualitative observations. In the nematic phase of *fd*, F-actin (Fig. 1a), wormlike micelles (Fig. 1b), and neurofilaments (Fig. 1c) are highly elongated, having a rod-like shape. By contrast, the same filaments dissolved in an isotropic phase crumple into more compact random coils. Just above the I-N transition, actin filaments and worm-like micelles form hairpin defects [9]. These hairpins exhibit interesting dynamics as shown in Fig. 1e, and will be explored by us in detail elsewhere. DNA dissolved in *fd* nematic behaves qualitatively differently (Fig. 1d); it forms a slightly anisotropic droplet. Each droplet contains many DNA molecules and, with time, these droplets coalesce into a larger droplet. Thus, even at a very low concentration, the DNA separates from the *fd* nematic. Taken together, these observations suggest that the persistence length of the polymer is important in determining its solubility in the nematic liquid crystals. DNA has a small ℓ_p and is insoluble unlike the other stiffer polymers in our experiments. This may be related to purely entropy-driven phase-separation of a system of bidisperse rigid rods if their lengths and/or diameters are sufficiently dissimilar [21]. This theory, however, has not been extended to the case of semi-flexible polymers.

The large contour lengths of actin filaments and worm-

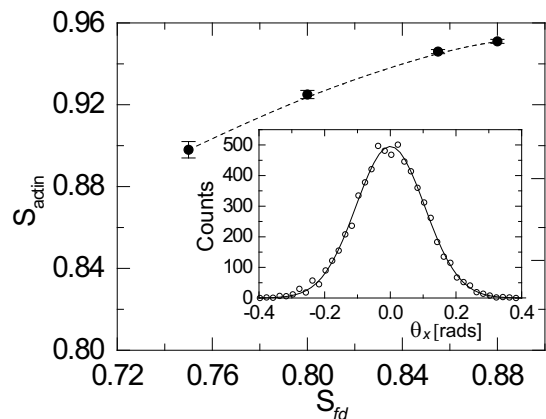


FIG. 2: The order parameter of actin filaments (S_{actin}) vs. the order parameter of the background *fd* nematic (S_{fd}). Dashed line is a guide to the eye. The contour length of actin filaments is $15 \mu\text{m}$ or higher. The values of S_{fd} at different *fd* concentration have been measured in Ref. [14]. Inset: The orientational distribution function (ODF) of wormlike micelles. The ODF is well approximated by a Gaussian distribution for a wide range of concentrations.

like micelles make them suitable for further quantitative analysis. We focus on the fluctuations of filaments in a background nematic that is free of both defects and distortions. A series of 50 to 100 images were taken with a few seconds between each image to ensure that statistically independent configurations were sampled. For each *fd* concentration, ten filaments were analyzed. The conformation of each polymer was reconstructed by manually marking the end points. (Note that we parameterize the transverse deviations of the polymer from the z axis by the 2-component vector $\mathbf{r}(z)$, as shown in Fig. 1f.) An intensity profile along the x direction for each value of z was extracted. By fitting this intensity to a Gaussian, we obtained sub-pixel accuracy for $r_x(z)$. We first extracted the orientational distribution function (ODF) from our data. Since our images are two dimensional projections of the polymer fluctuating in three dimensions, the x -component of the tangent vector is measured by $t_x(z) = \partial r_x(z)/\partial z \approx \theta_x(z)$. The ODF is obtained by creating a histogram of θ_x at different positions along the contour length for a time sequence of 50-100 images. The experimentally obtained ODF is plotted in Fig. 2a; it is well approximated by a Gaussian distribution.

Next, we compute the order parameter of the polymer defined by: $S \equiv \int_0^L dz \langle 3(\mathbf{t}(z) \cdot \hat{z})^2 - 1 \rangle / (2L) = 1 - 3\langle t_x^2(0) \rangle$, where in the last equality, we have used $\langle t_x^2(z) \rangle = \langle t_y^2(z) \rangle$. In Fig. 2, we plot S for actin as a function of the background nematic order parameter. It is interesting to observe that S_{actin} is significantly higher than S_{fd} . In order to check that the difference in the alignment between actin and *fd* molecules is due to their different contour lengths, we measured S_{actin} for different contour lengths of actin filaments, as shown in Fig. 3. As the contour length of actin decreases, S_{actin} approaches S_{fd} , as expected intuitively. These observations are qualitatively consistent with the Onsager theory for a bidisperse mixture of rod-like particles with different lengths

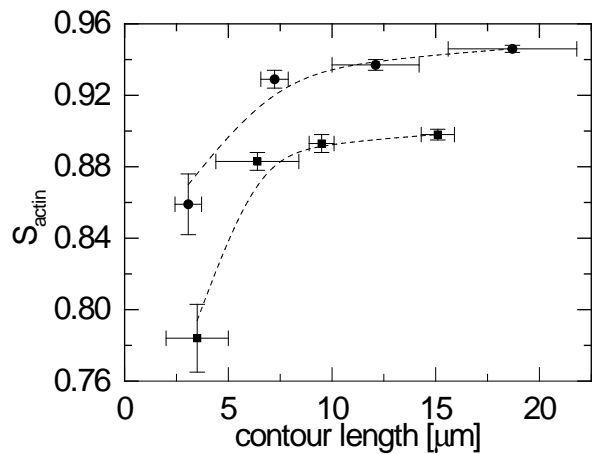


FIG. 3: S_{actin} vs. contour lengths of actin. The concentrations of the background nematic *fd* are 41 mg/ml (squares, $S_{fd} = 0.75$) and 28 mg/ml (circles, $S_{fd} = 0.855$). Dashed lines are a guide to the eye.

considered in Ref. [22]. This theory predicts the order parameter of long rods will be higher than the order parameter of the background nematic of shorter rods.

Finally, we measured the tangent-tangent correlation function (TTCF) $\langle t_x(z') t_x(z'+z) \rangle$ for wormlike micelles dissolved in *fd* virus with concentration 40 mg/ml and above (Fig. 4). At low *fd* concentrations, the fluctuations of worms are large as evidenced by visual observation of spontaneous formation and dissolution of hairpin defects. In this regime, the measured TTCF does not decay uniformly. We thus focus our analysis on the regime where the background order parameter is very high, and the amplitude of the polymer fluctuations is small. This makes our data suitable for comparison with the theoretical model outlined below.

The fluctuations of a semi-flexible polymer in a nematic phase may be described by the free energy [10, 23]:

$$F = \frac{k_B T}{2} \int_0^L dz \left\{ \ell_p \left[\frac{\partial \mathbf{t}_\perp}{\partial z} \right]^2 + \Gamma [\mathbf{t}_\perp(z) - \delta \bar{\mathbf{n}}(0, z)]^2 \right\} + \frac{1}{2} \int d^3x K (\nabla \delta \mathbf{n})^2, \quad (1)$$

where k_B is the Boltzmann constant, T is the temperature, ℓ_p is the persistence length of the semi-flexible polymer, Γ is the strength of the coupling of the polymer to the background nematic field, $\delta \mathbf{n}$ is the local direction of the fluctuating nematic field, and K is the nematic elastic constant. It is straightforward to compute $\langle t_x(z') t_x(z'+z) \rangle$ from Eq. (1):

$$\langle t_x(z') t_x(z'+z) \rangle = \frac{\lambda}{4\ell_p} e^{-z/\lambda} + \frac{1}{8\pi^2 K \lambda} \times \int_0^\infty dx \frac{\cos(xz/\lambda) \log(1 + D^2/x^2)}{(1+x^2) [1+x^2 + \frac{\Gamma x^2}{4\pi K} \log(1 + D^2/x^2)]}, \quad (2)$$

where $D = 2\pi\lambda/a$ is related to the molecular cutoff which we assume to be the diameter of the polymer ($a \sim 10$ nm). The first term in Eq. (2) describes the fluctuations of a semi-flexible polymer in a static external field, with a decaying length set by $\lambda = \sqrt{\ell_p/\Gamma}$. The second term describes the fluctuations of the polymers driven by the tight coupling to the fluctuations of the background nematic field. Note that this term generalizes that of Ref. [10], in that it includes the back reaction of the stiff polymer on the nematic fluctuations. Since it decays approximately as a power law, we expect at large lengthscales the fluctuations of the polymer are always dominated by the nematic fluctuations.

Figure 4 shows our measured TTCF along with the fitted curve of Eq. (2). Overall, good agreement is obtained at distances above $0.5 \mu\text{m}$ [24]. At these distances, most of the fluctuations of the worms are driven by the tight coupling to the background nematic field, coming from the second term in Eq. (2). The best-fit value of ℓ_p is found to be $1.5 \mu\text{m}$, somewhat higher than previous measurements [17]. From the fits to the data, we extract the values of the Odijk deflection length λ , K , and Γ ,

TABLE II: The Odijk deflection length λ , the elastic constant of the background nematic K , and the coupling constant between wormlike micelles and background nematic Γ for different fd concentrations obtained from the fits shown in Fig. 4. The persistence length of wormlike micelles that yield best fits is $1.5 \mu\text{m}$.

c_{fd} [mg/ml]	λ [μm]	K [10^{-8} dyne]	Γ [$1/\mu\text{m}$]
39	0.18	1.9	46
51	0.13	2.4	88
97	0.06	2.8	416

as listed in Table II. We observe that with increasing fd concentrations, λ decreases, while K and Γ increase, as one would intuitively expect. Finally, we note that the values for K are in agreement with previous measurements of twist elastic constant $K_{22} = 3 \cdot 10^{-8}$ dyne for fd samples prepared under similar conditions [25].

In conclusion, we have shown that semi-flexible polymers with large enough persistence lengths can be dissolved in a nematic background and then assume a rod-like conformation in this solvent. Using image analysis, a full nematic orientational distribution function was measured. In addition, we have also shown that the fluctuations of the polymer are driven primarily by the fluctuations of the background nematic field as has been predicted theoretically. Direct visualization of individual polymer yields valuable new information about the behavior of polymer chains in anisotropic solvents.

We thank Prof. Kamien for fruitful discussions. This work was supported by the NSF through grant DMR-

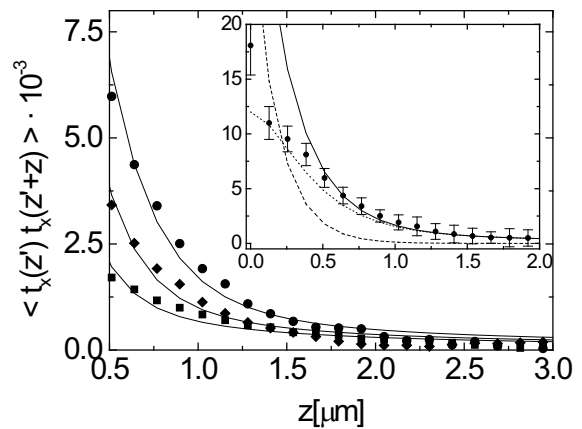


FIG. 4: The x component of the tangent-tangent correlation function for wormlike micelles measured at three different fd concentrations (c_{fd}). With increasing fd concentration the magnitude of the correlation function decreases. The solid lines are theoretical curves generated from Eq. (2) with the best-fit parameters listed in Table II. Inset: TTCF for the lowest concentration of the fd virus. The dashed and dotted lines are respectively the contributions of the first and second term in Eq. (2). The data points below $0.5 \mu\text{m}$ are unreliable and have been excluded from the fitting [24].

0203378 (AGY) and the MRSEC Grant DMR-0079909. We also gratefully acknowledge support from NASA NAG8-2172 (AGY) and the NIH R01 HL67286 (PAJ).

-
- [1] T.T. Perkins *et al.*, *Science* **268**, 83 (1995); D.E. Smith *et al.*, *Science* **283**, 1724 (1999); C.M. Schroeder *et al.*, *Science* **301**, 1515 (2003); C. Bustamante *et al.*, *Nature* **421**, 423 (2003).
- [2] J. Han and H.G. Craighead, *Science* **288**, 1026 (2000); D. Nykypanchuk *et al.*, *Science* **297**, 987 (2002).
- [3] M. Warner *et al.*, *J. Phys. A* **18**, 3007 (1985).
- [4] H. Finkelmann *et al.*, *Phys. Rev. Lett.* **87**, 015501 (2001).
- [5] P. Poulin *et al.*, *Science* **275**, 1770 (1997).
- [6] A. Bensimon *et al.*, *Science* **265**, 2096 (1994); V. Namiasivayam *et al.*, *Anal. Chem.* **74**, 3378 (2002).
- [7] R.A. Aldoroty *et al.*, *Biophys. J.* **51**, 371 (1987); N. Hirokawa *et al.*, *J. Cell. Biol.* **98**, 1523 (1984).
- [8] X.L. Ao and R.B. Meyer, *Physica A* **176**, 63 (1991); M.H. Li *et al.*, *Phys. Rev. Lett.* **70**, 2297 (1993); J.P. Cotton and F. Hardouin, *Prog. Poly. Sci.* **22**, 795 (1997).
- [9] P.-G. deGennes, in *Polymer Liquid Crystals*, edited by A. Ciferri, W.R. Krigbaum, and R.B. Meyer (Academic, New York, 1982).
- [10] R.D. Kamien *et al.*, *Phys. Rev. A* **45**, 8728 (1992); *Phys. Rev. E* **48**, 4119 (1993); P. LeDoussal and D.R. Nelson, *Europhys. Lett.* **15**, 161 (1992).
- [11] T. Odijk, *Macromolecules* **19**, 2313 (1986).
- [12] J. Tang and S. Fraden, *Liquid Crystals* **19**, 459 (1995).
- [13] Z. Dogic and S. Fraden, *Phil. Trans. R. Soc. Lond. A* **359**, 997 (2001).
- [14] K.R. Purdy *et al.*, *Phys. Rev. E* **67**, 031708 (2003).
- [15] L. Onsager, *Ann. N.Y. Acad. Sci.* **51**, 627 (1949).
- [16] J. F. Leterrier *et al.*, *J. Biol. Chem.* **271**, 15687, (1996).
- [17] P. Dalhaimer *et al.*, to be published.
- [18] M.D. Wang *et al.*, *Biophys. J.* **72**, 1335 (1997).
- [19] H. Aranda-Espinoza *et al.*, to be published.
- [20] A. Ott *et al.*, *Phys. Rev. E.* **48**, 1642 (1993); F. Gittes *et al.*, *J. Cell. Biol.* **120**, 923 (1993).
- [21] R. van Roij and B. Mulder, *J. Chem. Phys.* **105**, 11237 (1996).
- [22] H.N.W. Lekkerkerker *et al.*, *J. Chem. Phys.* **80**, 3427 (1984).
- [23] J.V. Selinger and R.F. Bruinsma, *Phys. Rev. A.* **43**, 2910 (1991).
- [24] At distances smaller than $0.5 \mu\text{m}$, we observe a significant deviation of our data from the theoretical curve, which likely arises from the limited spatiotemporal resolution of our microscope. Over the image acquisition time of 250 ms, the fast fluctuations of the polymers at short wavelengths are effectively washed out, leading a lower value in the TTCF. Another possible source of discrepancy is that the spatial resolution of the microscope is smaller than the Odijk deflection length.
- [25] Z. Dogic and S. Fraden, *Langmuir* **16**, 7820 (2000).